determined to be 10/*mmm*. Fig. 2.5.3.27(*d*) shows a CBED pattern taken by slightly tilting the incident beam to the *c** direction from incidence A. Dynamical extinction lines (arrowheads) are seen in the odd-order reflections along the *c** axis. This indicates the existence of a 10_5 screw axis and a *c*-glide plane. No other reflection absences were observed, implying the lattice type to be primitive. Therefore, the space group of $Al_{70}Ni_{20}Fe_{10}$ is determined to be centrosymmetric $P10_5/mmc$. It was found that the alloys with $0 \leq x \leq 7.5$ belong to the noncentrosymmetric space group $P\overline{1}0m2$ and those with $7.5 < x \leq 15$ belong to the centrosymmetric space group $P10_5/mmc$, keeping the specific polar structure of the basic clusters unchanged.

Another phase was found in the same alloys with $15 < x \leq 17$. This phase showed the same CBED symmetries as the phase with $7.5 < x \leq 15$. The space group of the phase was also determined to be $P10_5/mmc$. However, high-angle annular dark-field (HAADF) observations of the phase with $15 < x \leq 17$ showed that each atom cluster has only one mirror plane of symmetry (Saitoh *et al*., 1997, 1999). This implies that the structure of the specific cluster is changed from that of the phase with $7.5 < x \leq 15$. The clusters are still polar but take ten different orientations, producing centrosymmetric tenfold rotation symmetry on average, which was confirmed by HAADF observations (Saitoh, Tanaka & Tsai, 2001).

These three phases have been found for the similar alloys Al–*M*1–*M*2, where *M*1 = Ni and Cu, and *M*2 = Fe, Co, Rh and Ir (Tanaka *et al.*, 1996). Subsequently, decagonal quasicrystals were found in Al–Pd–Mn, Zn–Mg–RE (RE = Dy, Er, Ho, Lu, Tm and Y) and other alloy systems (Steurer, 2004). There are seven point groups in the decagonal system (Table 2.5.3.15). However, only two point groups, $\overline{1}0m2$ and 10/*mmm*, and two space groups, $P\overline{1}0m2$ and $P10_5/mmc$, are known reliably in real materials to date, though a few other point and space groups have been reported.

For further crystallographic aspects of quasicrystals, the reader is referred to the comprehensive reviews of Tsai (2003) and Steurer (2004), and to a review of more theoretical aspects by Yamamoto (1996).

2.5.4. Electron-diffraction structure analysis (EDSA)[2]

By B. K. Vainshtein and B. B. Zvyagin

2.5.4.1. Introduction

Electron-diffraction structure analysis (EDSA) (Vainshtein, 1964) based on electron diffraction (Pinsker, 1953) is used for the investigation of the atomic structure of matter together with X-ray and neutron diffraction analysis. The peculiarities of EDSA, as compared with X-ray structure analysis, are defined by a strong interaction of electrons with the substance and by a short wavelength λ. According to the Schrödinger equation (see Section 5.2.2) the electrons are scattered by the electrostatic field of an object. The values of the atomic scattering amplitudes, f_e, are three orders higher than those of X-rays, f_x, and neutrons, f_n. Therefore, a very small quantity of a substance is sufficient to obtain a diffraction pattern. EDSA is used for the investigation of very thin single-crystal films, of ~5–50 nm polycrystalline and textured films, and of deposits of finely grained materials and surface layers of bulk specimens. The structures of many ionic crystals, crystal hydrates and hydro-oxides, various inorganic, organic, semiconducting and metallo-organic compounds, of various minerals, especially layer silicates, and of biological structures have been investigated by means of EDSA; it has also been used in the study of polymers, amorphous solids and liquids.

Special areas of EDSA application are: determination of unit cells; establishing orientational and other geometrical relationships between related crystalline phases; phase analysis on the basis of d_{hkl} and I_{hkl} sets; analysis of the distribution of crystallite dimensions in a specimen and inner strains in crystallites as determined from line profiles; investigation of the surface structure of single crystals; structure analysis of crystals, including atomic position determination; precise determination of lattice potential distribution and chemical bonds between atoms; and investigation of crystals of biological origin in combination with electron microscopy (Vainshtein, 1964; Pinsker, 1953; Zvyagin, 1967; Pinsker *et al.*, 1981; Dorset, 1976; Zvyagin *et al.*, 1979).

There are different kinds of electron diffraction (ED) depending on the experimental conditions: high-energy (HEED) (above 30–200 kV), low-energy (LEED) (10–600 V), transmission (THEED) and reflection (RHEED). In electron-diffraction studies use is made of special apparatus – electron-diffraction cameras in which the lens system located between the electron source and the specimen forms the primary electron beam, and the diffracted beams reach the detector without aberration distortions. In this case, high-resolution electron diffraction (HRED) is obtained. ED patterns may also be observed in electron microscopes by a selected-area method (SAD). Other types of electron diffraction are: MBD (microbeam), HDD (high-dispersion), CBD (convergent-beam), SMBD (scanning-beam) and RMBD (rocking-beam) diffraction (see Sections 2.5.2 and 2.5.3). The recent development of electron diffractometry, based on direct intensity registration and measurement by scanning the diffraction pattern against a fixed detector (scintillator followed by photomultiplier), presents a new improved level of EDSA which provides higher precision and reliability of structural data (Avilov *et al*., 1999; Tsipursky & Drits, 1977; Zhukhlistov *et al*., 1997, 1998; Zvyagin *et al.*, 1996).

Electron-diffraction studies of the structure of molecules in vapours and gases is a large special field of research (Vilkov *et al*., 1978). See also *Stereochemical Applications of Gas-Phase Electron Diffraction* (1988).

2.5.4.2. The geometry of ED patterns

In HEED, the electron wavelength λ is about 0.05 Å or less. The Ewald sphere with radius λ^{-1} has a very small curvature and is approximated by a plane. The ED patterns are, therefore, considered as plane cross sections of the reciprocal lattice (RL) passing normal to the incident beam through the point 000, to scale $L\lambda$ (Fig. 2.5.4.1). The basic formula is

$$r = |\mathbf{h}|L\lambda, \text{ or } rd = L\lambda, \qquad (2.5.4.1)$$

where *r* is the distance from the pattern centre to the reflection, **h** is the reciprocal-space vector, *d* is the appropriate interplanar distance and *L* is the specimen-to-screen distance. The deviation of the Ewald sphere from a plane at distance *h* from the origin of the coordinates is $\delta_h = h^2\lambda/2$. Owing to the small values of λ and to the rapid decrease of f_e depending on $(\sin\theta)/\lambda$, the diffracted beams are concentrated in a small angular interval (≤ 0.1 rad).

Single-crystal ED patterns image one plane of the RL. They can be obtained from thin ideal crystalline plates, mosaic single-crystal films or, in the RHEED case, from the faces of bulk single crystals. Point ED patterns can be obtained more easily owing to the following factors: the small size of the crystals (increase in the dimension of RL nodes) and mosaicity – the small spread of crystallite orientations in a specimen (tangential tension of the RL nodes). The crystal system, the parameters of the unit cell and the Laue symmetry are determined from point ED patterns; the probable space group is found from extinctions. Point ED patterns may be used for intensity measurements if the kinematic

[2] Questions related to this section may be addressed to Dr D. L. Dorset (see list of contributing authors).

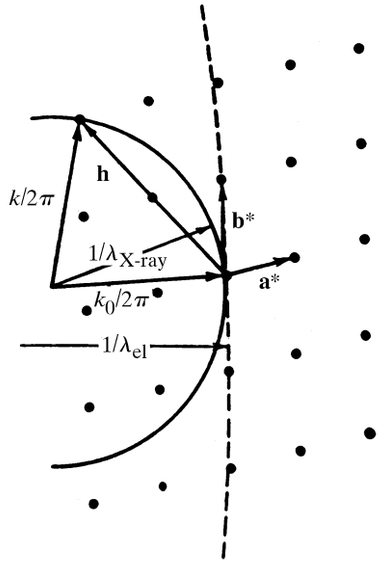

Fig. 2.5.4.1. Ewald spheres in reciprocal space. Dotted line: electrons, solid line: X-rays.

approximation holds true or if the contributions of the dynamic and secondary scattering are not too large.

The indexing of reflections and the unit-cell determination are carried out according to the formulae relating the RL to the DL (direct lattice) (Vainshtein, 1964; Pinsker, 1953; Zvyagin, 1967).

Under electron-diffraction conditions crystals usually show a tendency to lie down on the substrate plane on the most developed face. Let us take this as (001). The vectors **a** and **b** are then parallel, while vector $\mathbf{c}^*$ is normal to this plane, and the RL points are considered as being disposed along direct lines parallel to the axis c^* with constant hk and variable l.

The interpretation of the point patterns as respective RL planes is quite simple in the case of orthogonal lattices. If the lattice is triclinic or monoclinic the pattern of the crystal in the position with the face (001) normal to the incident beam does not have to contain $hk0$ reflections with nonzero h and k because, in general, the planes ab and a^*b^* do not coincide. However, the intersection traces of direct lines hk with the plane normal to them (plane ab) always form a net with periods

$$(a \sin\gamma)^{-1}, (b \sin\gamma)^{-1} \text{ and angle } \gamma' = \pi - \gamma \qquad (2.5.4.2a)$$

(Fig. 2.5.4.2). The points hkl along these directions hk are at distances

$$\eta = ha^* \cos\beta^* + kb^* \cos\alpha^* + lc^* \qquad (2.5.4.3)$$

from the ab plane.

By changing the crystal orientation it is possible to obtain an image of the a^*b^* plane containing $hk0$ reflections, or of other RL planes, with the exception of planes making a small angle with the axis c^*.

In the general case of an arbitrary crystal orientation, the pattern is considered as a plane section of the system of directions hk which makes an angle φ with the plane ab, intersecting it along a direction $[uv]$. It is described by two periods along directions $0h$, $0k$;

$$(a \sin\gamma \cos\psi_h)^{-1}, (b \sin\gamma \cos\psi_k)^{-1}, \qquad (2.5.4.2b)$$

with an angle γ'' between them satisfying the relation

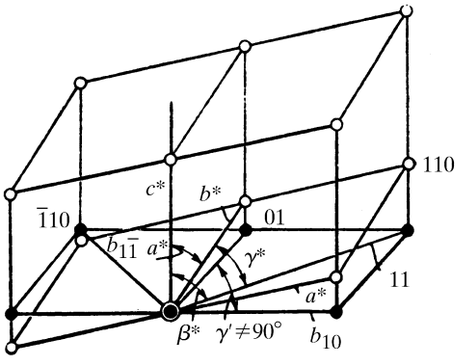

Fig. 2.5.4.2. Triclinic reciprocal lattice. Points: open circles, projection net: black circles.

$$\cos\gamma'' = \sin\psi_h \sin\psi_k - \cos\psi_h \cos\psi_k \cos\gamma, \qquad (2.5.4.2c)$$

and by a system of parallel directions

$$p_h h + p_k k = l; \quad l = 0, \pm1, \pm2, \ldots. \qquad (2.5.4.4)$$

The angles ψ_h, ψ_k are formed by directions $0h$, $0k$ in the plane of the pattern with the plane ab. The coefficients p_h, p_k depend on the unit-cell parameters, angle φ and direction $[uv]$. These relations are used for the indexing of reflections revealed near the integer positions hkl in the pattern and for unit-cell calculations (Vainshtein, 1964; Zvyagin, 1967; Zvyagin *et al.*, 1979).

In RED patterns obtained with an incident beam nearly parallel to the plane ab one can reveal all the RL planes passing through c^* which become normal to the beam at different azimuthal orientations of the crystal.

With the increase of the thickness of crystals (see below, Chapter 5.1) the scattering becomes dynamical and Kikuchi lines and bands appear. Kikuchi ED patterns are used for the estimation of the degree of perfection of the structure of the surface layers of single crystals for specimen orientation in HREM (*IT* C, 2004, Section 4.3.8). Patterns obtained with a convergent beam contain Kossel lines and are used for determining the symmetry of objects under investigation (see Section 2.5.3).

Texture ED patterns are a widely used kind of ED pattern (Pinsker, 1953; Vainshtein, 1964; Zvyagin, 1967). Textured specimens are prepared by substance precipitation on the substrate, from solutions and suspensions, or from gas phase in vacuum. The microcrystals are found to be oriented with a common (developed) face parallel to the substrate, but they have random azimuthal orientations. Correspondingly, the RL also takes random azimuthal orientations, having c^* as the common axis, *i.e.* it is a rotational body of the point RL of a single crystal. Thus, the ED patterns from textures bear a resemblance, from the viewpoint of their geometry, to X-ray rotation patterns, but they are less complicated, since they represent a plane cross section of reciprocal space.

If the crystallites are oriented by the plane (hkl), then the axis $[hkl]^*$ is the texture axis. For the sake of simplicity, let us assume that the basic plane is the plane (001) containing the axes a and b, so that the texture axis is $[001]^*$, *i.e.* the axis c^*. The matrices of appropriate transformations will define a transition to the general case (see *IT* A, 2005). The RL directions hk = constant, parallel to the texture axis, transform to cylindrical surfaces, the points with η_{hkl} = constant are in planes perpendicular to the texture axis, while any 'tilted' lines transform to cones or hyperboloids of rotation. Each point hkl transforms to a ring lying on these surfaces. In practice, owing to a certain spread of c^* axes of single crystals, the rings are blurred into small band sections of a

spherical surface with the centre at the point 000; the oblique cross section of such bands produces reflections in the form of arcs. The main interference curves for texture patterns are ellipses imaging oblique plane cross sections of the cylinders hk (Fig. 2.5.4.3).

At the normal electron-beam incidence (tilting angle $\varphi = 0^\circ$) the ED pattern represents a cross section of cylinders perpendicular to the axis c^*, *i.e.* a system of rings.

On tilting the specimen to an angle φ with respect to its normal position (usually $\varphi \simeq 60^\circ$) the patterns image an oblique cross section of the cylindrical RL, and are called oblique-texture (OT) ED patterns. The ellipses ($hk =$ constant) and layer lines ($l =$ constant) for orthogonal lattices are the main characteristic lines of ED patterns along which the reflections are arranged. The shortcoming of oblique-texture ED patterns is the absence of reflections lying inside the cone formed by rotation of the straight line coming from the point 000 at an angle $(90^\circ - \varphi)$ around the axis c^* and, in particular, of reflections $00l$. However, at $\varphi \lesssim 60$–70° the set of reflections is usually sufficient for structural determination.

For unit-cell determination and reflection indexing the values d (*i.e.* $|\mathbf{h}|$) are used, and the reflection positions defined by the ellipses hk to which they belong and the values η are considered. The periods a^*, b^* are obtained directly from h_{100} and h_{010} values. The period c^*, if it is normal to the plane a^*b^* (γ^* being arbitrary), is calculated as

$$c^* = \eta/l = (h_{hkl}^2 - h_{hk0}^2)^{1/2}/l. \qquad (2.5.4.5a)$$

For oblique-angled lattices

$$c^* = [(h_{l_1+l}^2 + h_{l_1-l}^2 - 2h_l^2)/2]^{1/2}/l. \qquad (2.5.4.5b)$$

In the general case of oblique-angled lattices the coaxial cylinders hk have radii

$$b_{hk} = (1/\sin\gamma)[(h^2/a^2) + (k^2/b^2) - (2hk\cos\gamma/ab)]^{1/2} \qquad (2.5.4.6)$$

and it is always possible to use the measured or calculated values b_{hk} in (2.5.4.5a) instead of h_{hk0}, since

$$\eta = (h_{hkl}^2 - b_{hk}^2)^{1/2}. \qquad (2.5.4.7)$$

In OT patterns the b_{hk} and η values are represented by the lengths of the small axes of the ellipses $B_{hk} = L\lambda b_{hk}$ and the distances of the reflections hkl from the line of small axes (equatorial line of the pattern)

$$D_{hkl} = L\lambda\eta/\sin\varphi = hp + ks + lq. \qquad (2.5.4.8)$$

Analysis of the B_{hk} values gives a, b, γ, while p, s and q are calculated from the D_{hkl} values. It is essential that the components of the normal projections c_n of the axis c on the plane ab measured in the units of a and b are

$$\begin{aligned} x_n &= (c/a)(\cos\beta - \cos\alpha\cos\gamma)/\sin^2\gamma \\ &= -p/q, \\ y_n &= (c/b)(\cos\alpha - \cos\beta\cos\gamma)/\sin^2\gamma \\ &= -s/q. \end{aligned} \qquad (2.5.4.9)$$

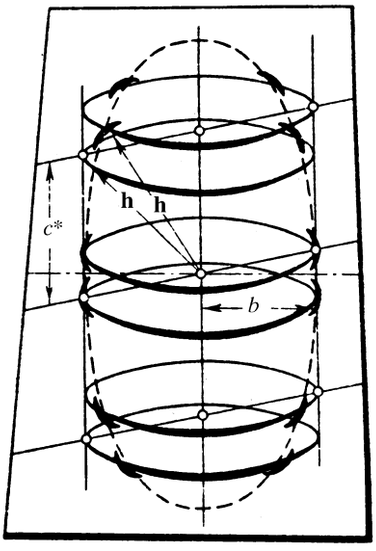

Fig. 2.5.4.3. Formation of ellipses on an electron-diffraction pattern from an oblique texture.

Obtaining x_n, y_n one can calculate

$$c_n = [(x_n a)^2 + (y_n b)^2 + 2x_n y_n ab\cos\gamma]^{1/2}.$$

Since

$$\begin{aligned} d_{001} &= L\lambda/q\sin\varphi, \\ c &= (c_n^2 + d_{001}^2)^{1/2}. \end{aligned} \qquad (2.5.4.10)$$

The α, β values are then defined by the relations

$$\begin{aligned} \cos\alpha &= (x_n a\cos\gamma + y_n b)/c, \\ \cos\beta &= (x_n a + y_n b\cos\gamma)/c. \end{aligned} \qquad (2.5.4.11)$$

Because of the small particle dimensions in textured specimens, the kinematic approximation is more reliable for OT patterns, enabling a more precise calculation of the structure amplitudes from the intensities of reflections.

Polycrystal ED patterns. In this case, the RL is a set of concentric spheres with radii h_{hkl}. The ED pattern, like an X-ray powder pattern, is a set of rings with radii

$$r_{hkl} = h_{hkl}L\lambda. \qquad (2.5.4.12)$$

2.5.4.3. Intensities of diffraction beams

The intensities of scattering by a crystal are determined by the scattering amplitudes of atoms in the crystal, given by (see also Section 5.2.1)

$$\begin{aligned} f_e^{abs}(s) &= 4\pi K\int \varphi(r)r^2\frac{\sin sr}{sr}\,dr; \\ K &= \frac{2\pi me}{h^2};\ f_e = K^{-1}f_e^{abs}, \end{aligned} \qquad (2.5.4.13)$$

where $\varphi(r)$ is the potential of an atom and $s = 4\pi(\sin\theta)/\lambda$. The absolute values of f_e^{abs} have the dimensionality of length L. In EDSA it is convenient to use f_e without K. The dimensionality of

f_e is [potential L^3]. With the expression of f_e in V Å^3 the value K^{-1} in (2.5.4.13) is 47.87 V Å^2.

The scattering atomic amplitudes $f_e(s)$ differ from the respective $f_x(s)$ X-ray values in the following: while $f_x(0) = Z$ (electron shell charge), the atomic amplitude at $s = 0$

$$f_e(0) = 4\pi \int \varphi(r) r^2 \, dr \qquad (2.5.4.14)$$

is the 'full potential' of the atom. On average, $f_e(0) \simeq Z^{1/3}$, but for small atomic numbers Z, owing to the peculiarities in the filling of the electron shells, $f_e(0)$ exhibits within periods of the periodic table of elements 'reverse motion', *i.e.* they decrease with Z increasing (Vainshtein, 1952, 1964). At large $(\sin\theta)/\lambda$, $f_e \simeq Z$. The atomic amplitudes and, consequently, the reflection intensities, are recorded, in practice, up to values of $(\sin\theta)/\lambda \simeq 0.8$–$1.2$ Å^{-1}, *i.e.* up to $d_{\min} \simeq 0.4$–0.6 Å.

The structure amplitude Φ_{hkl} of a crystal is determined by the Fourier integral of the unit-cell potential (see Chapter 1.2),

$$\Phi_{hkl} = \int_{\Omega} \varphi(\mathbf{r}) \exp\{2\pi i(\mathbf{r}\cdot\mathbf{h})\} \, dv_r, \qquad (2.5.4.15)$$

where Ω is the unit-cell volume. The potential of the unit cell can be expressed by the potentials of the atoms of which it is composed:

$$\varphi(\mathbf{r}) = \sum_{\text{cell},\, i} \varphi_{\text{at}\, i}(\mathbf{r} - \mathbf{r}_i). \qquad (2.5.4.16)$$

The thermal motion of atoms in a crystal is taken into account by the convolution of the potential of an atom at rest with the probability function $w(\mathbf{r})$ describing the thermal motion:

$$\varphi_{\text{at}} = \varphi_{\text{at}}(\mathbf{r}) * w(\mathbf{r}). \qquad (2.5.4.17)$$

Accordingly, the atomic temperature factor of the atom in a crystal is

$$f_{eT}[(\sin\theta)/\lambda] = f_e f_T = f_e[(\sin\theta)/\lambda] \exp\{-B[(\sin\theta)/\lambda]^2\}, \qquad (2.5.4.18)$$

where the Debye temperature factor is written for the case of isotropic thermal vibrations. Consequently, the structure amplitude is

$$\Phi_{hkl} = \sum_{\text{cell},\, i} f_{eT_i} \exp\{2\pi i(hx_i + ky_i + lz_i)\}. \qquad (2.5.4.19)$$

This general expression is transformed (see *IT* I, 1952) according to the space group of a given crystal.

To determine the structure amplitudes in EDSA experimentally, one has to use specimens satisfying the kinematic scattering condition, *i.e.* those consisting of extremely thin crystallites. The limit of the applicability of the kinematic approximation (Blackman, 1939; Vainshtein, 1964) can be estimated from the formula

$$A = \lambda \left| \frac{\langle \Phi_{\mathbf{h}} \rangle}{\Omega} \right| t \lesssim 1, \qquad (2.5.4.20)$$

where $\langle \Phi_{\mathbf{h}} \rangle$ is the averaged absolute value of $\Phi_{\mathbf{h}}$ (see also Section 2.5.2). Since $\langle \Phi_{\mathbf{h}} \rangle$ are proportional to $Z^{0.8}$, condition (2.5.4.20) is better fulfilled for crystals with light and medium atoms. Condition (2.5.4.20) is usually satisfied for textured and polycrystalline specimens. But for mosaic single crystals as well, the kinematic approximation limit is, in view of their real structure, substantially wider than estimated by (2.5.4.20) for ideal crystals. The fulfillment of the kinematic law for scattering can be, to a greater or lesser extent, estimated by comparing the decrease of experimental intensity $I_h[(\sin\theta)/\lambda]$ averaged over definite angular intervals, and sums $\sum f^2_{\text{obs}}[(\sin\theta)/\lambda]$ calculated for the same angular intervals.

For mosaic single-crystal films the integral intensity of reflection is

$$I_{\mathbf{h}} = j_0 S \lambda^2 \left| \frac{\Phi_{\mathbf{h}}}{\Omega} \right|^2 \frac{t d_{\mathbf{h}}}{\alpha} \simeq \Phi^2_{\mathbf{h}} d_{\mathbf{h}}; \qquad (2.5.4.21)$$

for textures

$$I_{\mathbf{h}} = j_0 S \lambda^2 \left| \frac{\Phi_{\mathbf{h}}}{\Omega} \right|^2 \frac{tL\lambda p}{2\pi R' \sin\varphi} \simeq \Phi^2_{\mathbf{h}} p / R'. \qquad (2.5.4.22)$$

Here j_0 is the incident electron-beam density, S is the irradiated specimen area, t is the thickness of the specimen, α is the average angular spread of mosaic blocks, R' is the horizontal coordinate of the reflection in the diffraction pattern and p is the multiplicity factor. In the case of polycrystalline specimens the local intensity in the maximum of the ring reflection

$$I_{\mathbf{h}} = j_0 S \lambda^2 \left| \frac{\Phi_{\mathbf{h}}}{\Omega} \right|^2 \frac{t d^2_{\mathbf{h}} p \Delta S}{4\pi L \lambda} \simeq \Phi^2_{\mathbf{h}} d^2_{\mathbf{h}} p \qquad (2.5.4.23)$$

is measured, where ΔS is the measured area of the ring.

The transition from kinematic to dynamic scattering occurs at critical thicknesses of crystals when $A \geq 1$ (2.5.4.20). Mosaic or polycrystalline specimens then result in an uneven contribution of various crystallites to the intensity of the reflections. It is possible to introduce corrections to the experimental structure amplitudes of the first strong reflections most influenced by dynamic scattering by applying in simple cases the two-wave approximation (Blackman, 1939) or by taking into account multibeam theories (Fujimoto, 1959; Cowley, 1981; Avilov *et al.* 1984; see also Chapter 5.2).

The application of kinematic scattering formulae to specimens of thin crystals (5–20 nm) or dynamic corrections to thicker specimens (20–50 nm) permits one to obtain reliability factors between the calculated Φ^{calc} and observed Φ^{obs} structure amplitudes of R = 5–15%, which is sufficient for structural determinations.

With the use of electron-diffractometry techniques, reliability factors as small as R = 2–3% have been reached and more detailed data on the distribution of the inner-crystalline potential field have been obtained, characterizing the state and bonds of atoms, including hydrogen (Zhukhlistov *et al.*, 1997, 1998; Avilov *et al.*, 1999).

The applicability of kinematics formulae becomes poorer in the case of structures with many heavy atoms for which the atomic amplitudes also contain an imaginary component (Shoemaker & Glauber, 1952). The experimental intensity measurement is made by a photo method or by direct recording (Avilov, 1979). In some cases the amplitudes Φ_{hkl} can be determined from dynamic scattering patterns – the bands of equal thickness from a wedge-shaped crystal (Cowley, 1981), or from rocking curves.

2.5.4.4. Structure analysis

The unit cell is defined on the basis of the geometric theory of electron-diffraction patterns, and the space group from extinc-

tions. It is also possible to use the method of converging beams (Section 2.5.3). The structural determination is based on experimental sets of values $|\Phi_{hkl}|^2$ or $|\Phi_{hkl}|$ (Vainshtein, 1964).

The trial-and-error method may be used for the simplest structures. The main method of determination is the construction of the Patterson functions

$$P(xyz) = \frac{1}{\Omega}\left[\Phi_{000}^2 + 2\sum_{hkl=-\infty}^{hkl=+\infty} |\Phi_{hkl}|^2 \cos 2\pi(hx + ky + lz)\right] \tag{2.5.4.24}$$

and their analysis on the basis of heavy-atom methods, superposition methods and so on (see Chapter 2.3). Direct methods are also used (Dorset *et al.*, 1979). Thus the phases of structure factors are calculated and assigned to the observed moduli

$$\Phi_{\mathbf{h}} = |\Phi_{\mathbf{h},\,\mathrm{obs}}| \exp\{i\alpha_{\mathrm{calc}}\}. \tag{2.5.4.25}$$

The distribution of the potential in the unit cell, and, thereby, the arrangement in it of atoms (peaks of the potential) are revealed by the construction of three-dimensional Fourier series of the potential (see also Chapter 1.3)

$$\varphi(xyz) = \frac{1}{\Omega}\sum_{\mathbf{h}} \Phi_{hkl} \exp\{-2\pi i(hx + ky + lz)\} \tag{2.5.4.26a}$$

or projections

$$\varphi'(xy) = \frac{1}{S}\sum_{\mathbf{h}} \Phi_{hk0} \exp\{-2\pi i(hx + ky)\}. \tag{2.5.4.26b}$$

The general formulae (2.5.4.26*a*) and (2.5.4.26*b*) transform, according to known rules, to the expressions for each space group (see *IT* I, 1952). If Φ_{hkl} are expressed in V Å^3 and the volume Ω or the cell area S in Å^3 and Å^2, respectively, then the potential φ is obtained directly in volts, while the projection of the potential φ' is in V Å. The amplitudes $|\Phi_{hkl}|$ are reduced to an absolute scale either according to a group of strong reflections

$$\sum|\Phi_{\mathbf{h}}|^{\mathrm{calc}} = \sum|\Phi_{\mathbf{h}}|^{\mathrm{obs}} \tag{2.5.4.27}$$

or using the Parseval equality

$$\sum_{\mathbf{h}=-\infty}^{+\infty} |\Phi_{\mathbf{h}}|^2 = \Omega^2\langle\varphi^2\rangle = \Omega\sum_{i(\mathrm{cell})} \frac{1}{2\pi^2}\int_0^{\infty} f_{eT_i}^2(s)\, s^2 \,\mathrm{d}s \tag{2.5.4.28}$$

or Wilson's statistical method

$$\langle\Phi^2[(\sin\theta)/\lambda]\rangle = \sum_i f_{eT_i}^2[(\sin\theta)/\lambda]. \tag{2.5.4.29}$$

The term Φ_{000} defines the mean inner potential of a crystal, and is calculated from $f_{\mathrm{e}}(0)$ [(2.5.4.13), (2.5.4.19)]

$$\langle\varphi_{\mathrm{cr}}\rangle = \Phi_{000}/\Omega = \frac{1}{\Omega}\sum f_{\mathrm{e}}(0). \tag{2.5.4.30}$$

The Fourier series of the potential in EDSA possess some peculiarities (Vainshtein, 1954, 1964) which make them different from the electron-density Fourier series in X-ray analysis. Owing to the peculiarities in the behaviour of the atomic amplitudes (2.5.4.13), which decrease more rapidly with increasing $(\sin\theta)/\lambda$ compared with f_{x}, the peaks of the atomic potential

$$\varphi_{\mathrm{at}}(r) = \frac{1}{2\pi^2}\int f_{eT}(s)\frac{\sin sr}{sr} s^2 \,\mathrm{d}s \tag{2.5.4.31}$$

are more 'blurred' and exhibit a larger half-width than the electron-density peaks $\rho_{\mathrm{at}}(r)$. On average, this half-width corresponds to the 'resolution' of an electron-diffraction pattern – about 0.5 Å or better. The potential in the maximum ('peak height') does not depend as strongly on the atomic number as in X-ray analysis:

$$\varphi(0) = \frac{1}{2\pi^2}\int f_{eT}(s)\, s^2 \,\mathrm{d}s \sim Z^{0.75}, \tag{2.5.4.32}$$

while in X-ray diffraction $\rho(0) \sim Z^{1.2}$. In such a way, in EDSA the light atoms are more easily revealed in the presence of heavy atoms than in X-ray diffraction, permitting, in particular, hydrogen atoms to be revealed directly without resorting to difference syntheses as in X-ray diffraction. Typical values of the atomic potential $\varphi(0)$ (which depend on thermal motion) in organic crystals are: H $\sim$ 35, C $\sim$ 165, O 215 V; in Al crystals 330 V, in Cu crystals 750 V.

The EDSA method may be used for crystal structure determination, depending on the types of electron-diffraction patterns, for crystals containing up to several tens of atoms in the unit cell. The accuracy in determination of atomic coordinates in EDSA is about 0.01–0.005 Å on average. The precision of EDSA makes it possible to determine accurately the potential distribution, to investigate atomic ionization, to obtain values for the potential between the atoms and, thereby, to obtain data on the nature of the chemical bond.

If the positions in the cell are occupied only partly, then the measurement of $\varphi_i(0)$ gives information on population percentage.

There is a relationship between the nuclear distribution, electron density and the potential as given by the Poisson equation

$$\nabla^2\varphi(\mathbf{r}) = -4\pi e[\rho_+(\mathbf{r}) - \rho_-(\mathbf{r})]. \tag{2.5.4.33}$$

This makes it possible to interrelate X-ray diffraction, EDSA and neutron-diffraction data. Thus for the atomic amplitudes

$$f_{\mathrm{e}}(s) = 4\pi Ke[Z - f_{\mathrm{x}}(s)]\, s^{-2}, \tag{2.5.4.34}$$

where Z is the nuclear charge and f_{x} the X-ray atomic scattering amplitude, and for structure amplitudes

$$\Phi_{hkl} = \pi Ke[Z_{hkl} - F_{hkl}]|\mathbf{h}|^{-2}, \tag{2.5.4.35}$$

where F_{hkl} is the X-ray structure amplitude of the electron density of a crystal and Z_{hkl} is the amplitude of scattering from charges of nuclei in the cell taking into account their thermal motion. The values Z_{hkl} can be calculated easily from neutron-diffraction data, since the charges of the nuclei are known and the experiment gives the parameters of their thermal motion.

In connection with the development of high-resolution electron-microscopy methods (HREM) it has been found possible to combine the data from direct observations with EDSA methods. However, EDSA permits one to determine the

atomic positions to a greater accuracy, since practically the whole of reciprocal space with 1.0–0.4 Å resolution is used and the three-dimensional arrangement of atoms is calculated. At the same time, in electron microscopy, owing to the peculiarities of electron optics and the necessity for an objective aperture, the image of the atoms in a crystal $\varphi'(\mathbf{x}) * A(\mathbf{x})$ is a convolution, with the aperture function blurring the image up to 1.5–2 Å resolution. In practice, in TEM one obtains only the images of the heaviest atoms of an object. However, the possibility of obtaining a direct image of a structure with all the defects in the atomic arrangement is the undoubted merit of TEM.

2.5.5. Image reconstruction[3]

By B. K. Vainshtein

2.5.5.1. Introduction

In many fields of physical measurements, instrumental and informative techniques, including electron microscopy and computational or analogue methods for processing and transforming signals from objects investigated, find a wide application in obtaining the most accurate structural data. The signal may be radiation from an object, or radiation transmitted through the object, or reflected by it, which is transformed and recorded by a detector.

The image is the two-dimensional signal $I(xy)$ on the observation plane recorded from the whole three-dimensional volume of the object, or from its surface, which provides information on its structure. In an object this information may change owing to transformation of the scattered wave inside an instrument. The real image $J(xy)$ is composed of $I(xy)$ and noise $N(xy)$ from signal disturbances:

$$J(xy) = I(xy) + N(xy). \tag{2.5.5.1}$$

Image-reconstruction methods are aimed at obtaining the most accurate information on the structure of the object; they are subdivided into two types (*Picture Processing and Digital Filtering*, 1975; Rozenfeld, 1969):

(*a*) Image restoration – separation of $I(xy)$ from the image by means of compensation of distortions introduced in it by an image-forming system as well as by an account of the available quantitative data reflecting its structure.

(*b*) Image enhancement – maximum exclusion from the observed image $J(xy)$ (2.5.5.1) of all its imperfections $N(xy)$ from both accidental distortions in objects and various 'noise' in signals and detector, and obtaining $I(xy)$ as the result.

These two methods may be used separately or in combination.

The image should be represented in the form convenient for perception and analysis, *e.g.* in digital form, in lines of equal density, in points of different density, in half-tones or colour form and using, if necessary, a change or reversal of contrast.

Reconstructed images may be used for the three-dimensional reconstruction of the spatial structure of an object, *e.g.* of the density distribution in it (see Section 2.5.6).

This section is connected with an application of the methods of image processing in transmission electron microscopy (TEM). In TEM (see Section 2.5.2), the source-emitted electrons are transmitted through an object and, with the aid of a system of lenses, form a two-dimensional image subject to processing.

Another possibility for obtaining information on the structure of an object is structural analysis with the aid of electron diffraction – EDSA. This method makes use of information in reciprocal space – observation and measurement of electron-diffraction patterns and calculation from them of a two-dimensional projection or three-dimensional structure of an object using the Fourier synthesis. To do this, one has to find the relative phases of the scattered beams.

The wavefunction of an electron-microscopic image is written as

$$\psi_\mathrm{I} = \mathscr{F}^{-1} T \mathscr{F} q \psi_0. \tag{2.5.5.2}$$

Here ψ_0 is the incident plane wave. When the wave is transmitted through an object, it interacts with the electrostatic potential $\varphi(\mathbf{r})$ [$\mathbf{r}(xyz)$ is the three-dimensional vector in the space of the object]; this process is described by the Schrödinger equation (Section 2.5.2.1). As a result, on the exit surface of an object the wave takes the form $q\psi_0(\mathbf{x})$ where q is the transmission function and $\mathbf{x}$ is the two-dimensional vector $\mathbf{x}(xy)$. The diffraction of the wave $q\psi_0$ is described by the two-dimensional Fourier operator:

$$\mathscr{F} q = Q(\mathbf{u}) = \int q(\mathbf{x}) \exp[2\pi i(\mathbf{x}\mathbf{u})]\, \mathrm{d}\mathbf{x}. \tag{2.5.5.3}$$

Here, we assume the initial wave amplitude to be equal to unity and the initial phase to be zero, so that $q\psi_0 = q$, which defines, in this case, the wavefunction in the back focal plane of an objective lens with the reciprocal-space coordinates $\mathbf{u}(u, v)$. The function Q is modified in reciprocal space by the lens transfer function $T(\mathbf{u})$. The scattered wave transformation into an image is described by the inverse Fourier operator $\mathscr{F}^{-1}TQ$.

The process of the diffraction $\mathscr{F} q\psi_0 = Q$, as seen from (2.5.5.1), is the same in both TEM and EDSA. Thus, in TEM under the lens actions $\mathscr{F}^{-1}TQ$ the image formation from a diffraction pattern takes place with an account of the phases, but these phases are modified by the objective-lens transfer function. In EDSA, on the other hand, there is no distorting action of the transfer function and the 'image' is obtained by computing the operation $\mathscr{F}^{-1}Q$.

The computation of projections, images and Fourier transformation is made by discretization of two-dimensional functions on a two-dimensional network of points – pixels in real space $\mathbf{x}(x_j, y_k)$ and in reciprocal space $\mathbf{u}(u_m, v_n)$.

2.5.5.2. Thin weak phase objects at optimal defocus

The intensity distribution $I(xy) \sim |\psi_1|^2$ of an electron wave in the image plane depends not only on the coherent and inelastic scattering, but also on the instrumental functions. The electron wave transmitted through an object interacts with the electrostatic potential $\varphi(\mathbf{r})$ which is produced by the nuclei charges and the electronic shells of the atoms. The scattering and absorption of electrons depend on the structure and thickness of a specimen, and the atomic numbers of the atoms of which it is composed. If an object with the three-dimensional distribution of potential $\varphi(\mathbf{r})$ is sufficiently thin, then the interaction of a plane electron wave ψ_0 with it can be described as the interaction with a two-dimensional distribution of potential projection $\varphi(\mathbf{x})$,

$$\varphi(\mathbf{x}) = \int_0^b \varphi(\mathbf{r})\, \mathrm{d}z, \tag{2.5.5.4}$$

where b is the specimen thickness. It should be noted that, unlike the three-dimensional function of potential $\varphi(\mathbf{r})$ with dimension $[M^{1/2}L^{3/2}T^{-1}]$, the two-dimensional function of potential projection $\varphi(\mathbf{x})$ has the potential-length dimension $[M^{1/2}L^{1/2}T^{-1}]$ which, formally, coincides with the charge dimension. The transmission function, in the general case, has the form

[3] Questions related to this section may be addressed to Dr P. A. Penczek (see list of contributing authors).